International Journal of Scientific Research in Science and Technology
Print ISSN: 2395-6011 | Online ISSN: 2395-602X (www.ijsrst.com)
doi : https://doi.org/10.32628/IJSRST2293148

Development of Helmholtz Equation of State for Thermodynamic Properties of R-1233zd(E)

Galih Budiarso[1], I Made Astina[2,3]
[1]PT Pupuk Kalimantan Timur, Indonesia
[2]Faculty of Mechanical and Aerospace Engineering, Institut Teknologi Bandung, Indonesia
[3]Corresponding Author's Email: astina@ftmd.itb.ac.id

Article Info
Volume 9, Issue 3
Page Number: 765–776

Publication Issue
May-June-2022

Article History
Accepted: 20 June 2022
Published: 28 June 2022

ABSTRACT

The application of refrigerants from the Hydro Chloro Fluoro Olefins (HCFO) group, namely R-1233zd(E), in addition to the Hydro Fluoro Olefins (HFO), is a solution to environmental problems. A thermodynamic equation of state for R-1233zd(E), which can predict all thermodynamic properties over a wide-range fluid phase, is proposed in a function of the Helmholtz free energy. Three ancillary equations support the development and application. A genetic algorithm method combined with a weighted least squares regression was applied. The Helmholtz equation of state has an average absolute deviation of 0.12% for the liquid density, 2.0% for the vapor density, 1.4% for the vapor pressure, 0.16% for the saturated liquid density, 4.1% for the saturated vapor density, 3.6% for the isobaric specific heat, and 0.15% for the speed of sound in the liquid phase, and 0.18% for the speed of sound in the vapor phase. The deviation of the isochoric and saturated specific heats was not evaluated yet due to unavailable experimental data. The reasonable behavior of its extrapolation and ideal characteristic curves confirm its reliability. The Helmholtz equation of state can predict thermodynamic properties from the triple point to 1000 K and 100 MPa.

Keywords: Helmholtz Equation of State, Trans-1-Chloro-3,3,3-Trifluoropropene, Thermodynamic Properties

I. INTRODUCTION

The development of air conditioning and refrigeration technology consists of equipment, refrigerants, and a thermodynamic cycle. The development is necessary for improving the quality of working fluid and system performance. The quality of the refrigerant affects the system's performance and its environmental impact. Air conditioner manufacturers are currently very concerned about refrigerants to produce environmentally friendly technologies. Despite its enormous benefits, refrigerants harm their use. A negative impact causes global warming and ozone layer depletion called an environmental issue. The emergence of these two problems is a motivating factor for the search for alternative refrigerants. The use of refrigerants in air conditioning and refrigeration systems is considered dangerous for the continuity of the ozone production cycle in the atmosphere.

Global warming issues have led to efforts to reduce the using potentially global warming substances (GWP) for engineering and consumption of fossil fuels. Hydro Fluoro Olefins (HFOs) and Hydro Chloro Fluoro Olefins (HCFOs) are disruptive technologies to bridge the historical gap between maximizing safety and minimizing GWP. Using non-flammable, low toxicity level for Hydro Fluoro Carbon (HFC) but high GWP can achieve high safety. In contrast, the minimum GWP is achieved when using hydrocarbons but is highly flammable. Likewise, ammonia is toxic. The available HFO and HCFO have various physical properties that allow optimal options for widely varying applications, but never for carbon dioxyde [1]. R-1233zd(E) is suitable for chiller applications, high temperature heat pumps, working fluid for organic Rankine cycle, blowing agent for insulation foams, and precision solvents [2]. R-1233zd(E) centrifugal chillers from 3 different manufacturers have received environment awards in the world for their class-leading performance, making them ideal for low pressure centrifugal chillers delivering high efficiencies [3]. It is non-flammable and has a slighter odor with poor warning properties [4].

II. DATA AND SELECTION

Trans-1-chloro-3,3,3-trifluoropropene ($C_3H_2ClF_3$) known as R-1233zd(E) is included in the HCFO refrigerant group, which is composed of 3 carbon atoms, 2 hydrogen atoms, 3 fluorine atoms, and 1 chlorine atom with double bonds on carbon atoms. This refrigerant is also called as HCFO-1233zd(E). The two sides of the double bond contain hydrogen in opposite positions so trans is added to the naming under the IUPAC. E in parentheses refers to the ASHRAE standard indicating the hydrogen atoms in opposite positions. R-1233zd(E) has a GWP value of one and an ODP of zero [5].

A factor that affects the accuracy and reliability of an equation of state (EOS) is input data in the modeling process. The data quality significantly depends on the uncertainty, accuracy, amount, density, and distribution. The data quality affects the reliability of EOS in predicting the ther-modynamic properties over a wide-range fluid. R-1233zd(E) is a new refrigerant with few available experimental data. The input data covers the liquid and vapor phases, supercritical region, and saturation. The experimental data used are critical point, triple point, pressure-density-temperature ($p\rho T$), isobaric specific heat (c_p), isochoric specific heat (c_v), and speed of sound (w). Analytical data based on the mathematical relationships, which are the ideal-gas isobaric specific heat (c_p^0), the second virial coefficient (B), and the third virial coefficient (C) are also included.

Two sources of the experimental data for a critical point are currently available. Both sources are the data results of the study of Hulse et al. [6] and Mondejar et al. [7]. Data of Mondejar et al. is selected since the fluid purity is higher than the fluid of Hulse et al. Mondejar et al. used the purity of 99.985%, while Hulse et al. used the purity of 99%. The critical point chosen is 439.6 K of the critical temperature (T_c), 3.6237 MPa of the critical pressure (p_c), and 480.2194 kg·m^{-3} of the critical density (ρ_c) [7]. The triple point 195.15 K is taken from the study result conducted by Zhang et al. [8] and the molecular mass is 130.4960 g·mol^{-1} [9]. Universal gas constant is 8.314462618 J·mol^{-1}·K^{-1} [10]. Most available data collected from this literature study appear in Table 1. The data collected into three groups are ideal gas, $p\rho T$, and caloric data.

Trans-1-chloro-3,3,3-trifluoropropene ($C_3H_2ClF_3$) known as R-1233zd(E) is included in the HCFO refrigerant group, which is composed of 3 carbon atoms, 2 hydrogen atoms, 3 fluorine atoms, and 1 chlorine atom with double bonds on carbon atoms. This refrigerant is also called as HCFO-1233zd(E). The two sides of the double bond contain hydrogen in opposite positions so trans is added to the naming under the IUPAC. E in parentheses refers to the ASHRAE standard indicating the hydrogen atoms in opposite positions. R-1233zd(E) has a GWP value of one and an ODP of zero [5].

Table 1. Available data of R-1233zd(E)

No	Source	Property	Total	Temperature range (K)	Purity
1	Hulse et al. [6]	c_p^o	11	100–1000	-
2	Hulse et al. [6]	p_s	16	263.09–352.84	99%
3	Mondejar et al. [7]	p_s	23	280.009–437.909	99.985%
4	Nicola et al. [11]	p_s	81	234.15–437.91	99.5%
5	Raabe [12]	p_s	8	273.15–383.15	-
6	Hulse et al. [6]	ρ'	13	243.34–293.21	99%
7	Raabe [12]	ρ'	8	273.15–383.15	-

No	Source	Property	Total	Temperature range (K)	Purity
8	Raabe [12]	ρ''	8	273.15–383.15	-
9	Mondejar et al. [7]	$p\rho T$	161	215.006–443.947	99.985%
10	Tanaka [13]	$p\rho T$	97	328.5–443.54	99.5%
11	Fedele et al. [14]	$p\rho T$	154	283.14–373.15	99.5%
12	Romeo et al. [15]	$p\rho T$	30	274.147–333.152	-
13	Liu and Zhao [16]	c_p	63	313.277–445.857	99.95%
14	Mondejar et al. [7]	w	155	289.991–419.695	99.985%
15	Lago et al [17]	w	43	273.15–353.15	99.5%

The first data group is ideal-gas data that play an essential role in developing an ideal part of the EOS due to separating ideal-gas properties from real-fluid properties by introducing departure properties. This concept is existed to develop or derive caloric properties from an EOS explicitly represented in $p\rho T$ relation. The ideal-gas isobaric specific-heat can be derived from an analytic relationship to the speed-of-sound experimental data. Hulse et al. [6] reported the equation to complement these specific-heat data for a temperature range of 100–1000 K with 11 points of data. The second data group is $p\rho T$ at a saturation state and in a single phase. Saturation data consisting of the vapor pressure (p_s), saturated temperature (T_s), saturated liquid density (ρ'), and saturated vapor density (ρ'') are necessary for the modeling process. The saturation data were used as input to develop ancillary equations. The data distrubution of $p\rho T$ in the single phase is shown in Fig. 1. The third data group is caloric data. As indicated in Table 1 and Fig. 2, available data on caloric properties are very scarce. These data are essential in multi-property regression. The speed-of-sound data involved in improving a reliable and accurate EOS were used for developing the residual part.

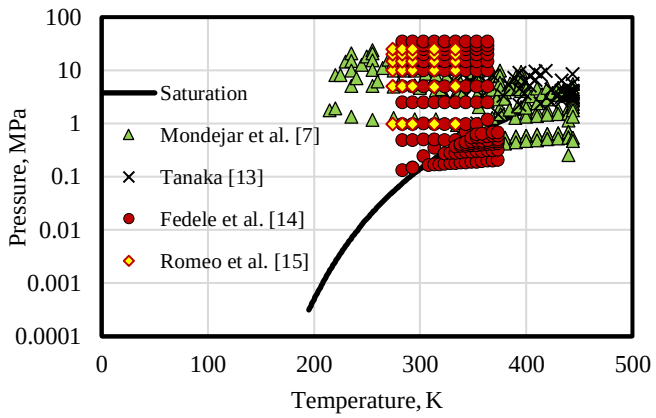

Fig. 1. Data distribution of $p\rho T$ in the single phase

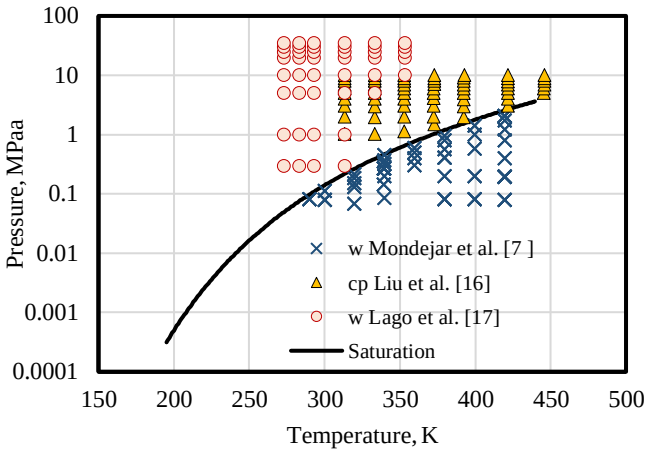

Fig. 2. Caloric data distribution in the single phase

III. MODELLING AND ASSESSMENT METHODS

The EOS developed is through three stages. The stages are the formulation and optimization of the ancillary equations, the ideal-gas isobaric specific-heat equation, and the residual part of the EOS. The ancillary equations and the ideal-gas specific-heat equation have a function of temperature, while the residual part has a function of temperature and density.

The genetic algorithm combined with weighted least squares regression was used for getting the ancillary equations and EOS. This optimization procedure was comprehensively explained in our previous paper [19] and applied for various refrigerants such as HFC, hydrocarbon, and HFO [20]. Principally, nonlinear constants in the equation are introduced from a genetic algorithm. The linear related coefficients are calculated from the weighted least squares regression. Among relations of each property in Table 2 included in regression are expressed in weighted least squares by multiplying a weighted factor with deviation squares between the left term values from the input data and the calculated values from the right term for the same point data. The sum of the weighted least squares of the deviation for properties included in the optimization is used as fitness in the genetic algorithm. Similarly, each ancillary equation is expressed in the weighted least squares by multiplying a weighted factor with deviation squares between the dependent property values from the input data and the calculated values from the equation for the same point data.

Table 2. Relation of thermodynamic properties

Property	Thermodynamic relations
Ideal gas isobaric specific heat	$\frac{c_p^0}{R} = 1 - \tau^2 \alpha_{\tau\tau}^0 = 1 + \frac{c_v^0(\tau)}{R}$
Pressure	$\frac{p(\delta,\tau)}{\rho RT} = 1 + \delta \alpha_\delta^r$
Vapor pressure	$\frac{p_s(\delta',\delta'',\tau_s)}{RT_s} = \frac{\rho'\rho''}{\rho'-\rho''}\left(\ln\left(\frac{\delta'}{\delta''}\right) + \alpha^{r\prime} - \alpha^{r\prime\prime}\right)$
Third virial coefficient	$B(\tau)\rho_c = \lim_{\delta\to 0} \alpha_\delta^r$
Second virial coefficient	$C(\tau)\rho_c^2 = \lim_{\delta\to 0} \alpha_{\delta\delta}^r$
Isobaric specific heat	$\frac{c_p(\delta,\tau)}{R} = \frac{c_v(\delta,\tau)}{R} + \frac{(1+\delta\alpha_\delta^r - \delta\tau\alpha_{\delta\tau}^r)^2}{(1+2\delta\alpha_\delta^r + \delta^2\alpha_{\delta\delta}^r)}$
Isochoric specific heat	$c_v(\delta,\tau)/R = -\tau^2(\alpha_{\tau\tau}^0 + \alpha_{\tau\tau}^r)$
Speed of Sound	$\frac{w^2(\delta,\tau)M}{RT} = 1 + 2\delta\alpha_\delta^r + \delta^2\alpha_{\delta\delta}^r + \frac{(1+\delta\alpha_\delta^r - \delta\tau\alpha_{\delta\tau}^r)^2}{c_v(\delta,\tau)/R}$
Saturated liquid specific heat	$\frac{c_s{}'(\delta',\delta'',\tau_s)}{R} = \frac{c_v(\delta',\tau_s)}{R} + \frac{(1+\delta'\alpha_\delta^{r\prime} - \delta'\tau_s\alpha_{\delta\tau}^{r\prime})}{(1+2\delta'\alpha_\delta^{r\prime} + \delta'^2\alpha_{\delta\delta}^{r\prime})} \times \left\{1 + \delta'\alpha_\delta^{r\prime} - \delta'\tau_s\alpha_{\delta\tau}^{r\prime} - \frac{1}{R\rho_c\delta'}\frac{dp_s(\delta',\delta'',\tau_s)}{dT}\right\}$
Saturated vapor specific heat	$\frac{c_s{}''(\delta',\delta'',\tau_s)}{R} = \frac{c_v(\delta'',\tau_s)}{R} + \frac{(1+\delta''\alpha_\delta^{r\prime} - \delta''\tau_s\alpha_{\delta\tau}^{r\prime})}{(1+2\delta''\alpha_\delta^{r\prime} + \delta''^2\alpha_{\delta\delta}^{r\prime})} \times \left\{1 + \delta''\alpha_\delta^{r\prime} - \delta''\tau_s\alpha_{\delta\tau}^{r\prime} - \frac{1}{R\rho_c\delta''}\frac{dp_s(\delta',\delta'',\tau_s)}{dT}\right\}$
Internal energy	$\frac{u(\delta,\tau)}{RT} = \tau(\alpha_\tau^0 + \alpha_\tau^r)$
Enthalpy	$\frac{h(\delta,\tau)}{RT} = \tau(\alpha_\tau^0 + \alpha_\tau^r) + 1 + \delta\alpha_\delta^r$
Entropy	$\frac{s(\delta,\tau)}{R} = \tau(\alpha_\tau^0 + \alpha_\tau^r) - (\alpha^0 + \alpha^r)$
$\alpha_\delta = \left(\frac{\partial\alpha}{\partial\delta}\right)_\tau$, $\alpha_\tau = \left(\frac{\partial\alpha}{\partial\tau}\right)_\delta$, $\alpha_{\delta\delta} = \left(\frac{\partial^2\alpha}{\partial\delta^2}\right)_\tau$, $\alpha_{\tau\tau} = \left(\frac{\partial^2\alpha}{\partial\tau^2}\right)_\delta$, $\alpha_{\delta\tau} = \left(\frac{\partial^2\alpha}{\partial\delta\partial\tau}\right)$, $\delta = \frac{\rho}{\rho_c}$, $\tau = \frac{T_c}{T}$	

The ideal part cannot be directly developed in the formulation and optimization but established using an integral process of the ideal-gas isobaric specific heat equation. Formulation and optimization of the ideal-gas isobaric specific-heat equation are essential to get an accurate ideal part, which is increasingly reliable. The equation accuracy also influences the calculation values of caloric properties.

The modeling of the residual part involves the density of single phase, vapor pressure, saturated liquid density, saturated vapor density, isochoric density, isobaric density, saturated density, and speed of sound. The second and third virial coefficient data are also included in the modeling. The multi-property regression and formulation optimization process applied causes the work to be more complicated. The complexity arises since more than one objective function is used in the modeling process. The thermodynamic nature of one also affects the other thermodynamic properties.

The deviation is a relative value represented in percent, which is a comparison of the property value derived from the equation to the experimental data or other existing equations as defined in Eq. 1. A small deviation value indicates that the equation has high accuracy, whereas a large deviation means that the equation has low accuracy. Each property is assessed for finding statistical parameters. The parameters consist of the average absolute deviation (AAD), the average deviation (BIAS), the standard deviation (STD), and the maximum absolute deviation (MAX). All of these parameters have relations as written in Eqs. 1–4.

$$\Delta = \frac{Y - Y_{cal}}{Y_{cal}} \cdot 100\% \quad (1)$$

$$AAD = \frac{1}{N}\sum_{i=1}^{N} |\Delta_i| \quad (2)$$

$$BIAS = \frac{1}{N}\sum_{i=1}^{N} \Delta_i \quad (3)$$

$$STD = \sqrt{\frac{1}{N-1}\sum_{i=1}^{N} (\Delta_i - BIAS)^2} \quad (4)$$

IV. MODELING RESULTS

Modeling results consist of the Helmholtz EOS and three ancillary equations. The main focus of the modeling is to establish the EOS. However, the ancillary equations, which are an essential function in the EOS development and implementation, is included in this section.

A. Ancillary Equations of Saturation Properties

The ancillary equations developed in this study consist of the vapor pressure (p_s), the saturated liquid density (ρ'), and the saturated vapor density (ρ") equations as written in Eqs. 4–6. The equations have a function in dimensionless by using critical parameters of critical temperature (T_c), critical pressure (p_c), and critical density (ρ_c). The numerical coefficients and exponents for the equations are listed in Table 3. Deviation visualization for each equation is indicated simultaneously for assessing the new EOS.

$$\ln(p_s/p_c) = (T_c/T)\sum_{i=1}^{4} K_i(1-T/T_c)^{k_i} \quad (4)$$

$$\rho'/\rho_c = 1 + \sum_{i=1}^{4} L_i\,(1-T/T_c)^{l_i} \quad (5)$$

$$\ln(\rho''/\rho_c) = \sum_{i=1}^{4} N_i\,(1-T/T_c)^{n_i} \quad (6)$$

Table 3. Coefficients and exponents in Eqs. 4–6

i	k_i	K_i	l_i	L_i	n_i	N_i
1	0.6	1.1391	0.5	7.3155	0.5	-4.6558
2	0.8	-5.7033	0.6	-5.4525	1.9	-11.959
3	1.5	-2.8522	1.2	0.93249	4.7	-34.273
4	6	-6.9428	5.7	0.47074	9.1	-80.653

B. New Helmholtz Equation of State

EOS (α) is represented in dimensionless form by reducing Helmholtz free energy (A) with a gas constant (R) and temperature (T). The EOS is given in two parts: an ideal part (α^o) and a residual part (α^r) so that the EOS is summation of the ideal part and residual part. Each part consists of independent parameters of dimensionless density and temperature symbolized in δ and τ, respectively. The δ is a ratio of densities to the critical density, and the τ is a ratio of the critical temperature to temperatures. The EOS was finally established by taking a reference state under International Institute of Refrigeration (IIR) using enthalpy of 200 kJ·kg^{-1} and entropy of 1 kJ·kg^{-1}·K^{-1} at a saturated liquid of 273.15 K.

The ideal part can be established by integrating an ideal-gas isobaric specific-heat (c_p^o) equation. Its structural form was simultaneously optimized with our recently previous work for R-1234ze(E) [20]. The specific heat is reduced by a gas constant to make a dimensionless as written in Eq. 7. The integral process yields the ideal part, and it is finally fitted to a reference state after the residual part was established. The final ideal part is written in Eq. 8 with numerical coefficients and constants listed in Table 4.

$$\frac{c_p^o(\tau)}{R} = \sum_{i=3}^{5} N_i^o \tau^2 b_i^2 \frac{\exp(-b_i\,\tau)}{\left(1-\exp(-b_i\,\tau)\right)^2} \quad (7)$$

$$\alpha^o(\delta,\tau) = \ln\frac{\delta}{\tau} + \sum_{i=1}^{2} N_i^o\,\tau^{b_i} + \sum_{i=3}^{5} N_i^o \ln\left(1-\exp(-b_i\,\tau)\right) \quad (8)$$

Table 4. Coefficients and constants of the Eqs. 7 and 8

i	b_i	N_i^o
1	0	-8.5461639
2	1	9.8378490
3	0.3895	8.6070194
4	2.1662	9.1046764
5	4.9593	6.2980225

The residual part of the EOS as a result of this study is written in Eq. 9. Its structural form was also simultaneously optimized with previous work for HFO-1234ze(E) [20]. The numerical coefficients and exponents contained in each term of the part are written in Table 6. The EOS consists of 17 terms, while the residual part of Mondejar et al. [7] has 15 terms.

$$\alpha^r(\delta,\tau) = \sum_{i=1}^{8} N_i\delta^{d_i}\tau^{t_i} + \sum_{i=9}^{13} N_i\delta^{d_i}\tau^{t_i}\exp\left[-\delta^{\theta_i}\right] + \sum_{i=14}^{17} N_i\delta^{d_i}\tau^{t_i}\exp\left[-\beta_i(\delta-\epsilon_i)^{\theta_i} - \gamma_i(\tau-\mu_i)^{\varphi_i}\right] \quad (9)$$

Table 5. Coefficients and constants of the residual part

i	d_i	t_i	β_i	ϵ_i	θ_i	γ_i	μ_i	φ_i	N_i
1	1	0.223	-	-	-	-	-	-	1.3619999×10^{00}
2	1	0.755	-	-	-	-	-	-	-1.4246278×10^{00}
3	2	0.85	-	-	-	-	-	-	8.7814082×10^{00}
4	2	0.95	-	-	-	-	-	-	-1.1297612×10^{01}
5	2	1.24	-	-	-	-	-	-	2.1071241×10^{00}
6	4	1.1	-	-	-	-	-	-	6.1446972×10^{-02}
7	4	1.75	-	-	-	-	-	-	-1.7909249×10^{-02}

i	d_i	t_i	β_i	ϵ_i	θ_i	γ_i	μ_i	φ_i	N_i
8	4	2.535	-	-	-	-	-	-	4.3764884×10^{-03}
9	1	2.06	1	-	1	-	-	-	-1.0010770×10^{00}
10	1	1.95	1	-	2	-	-	-	-2.7836201×10^{-01}
11	2	7.45	1	-	2	-	-	-	-1.1747803×10^{-01}
12	3	2.97	1	-	1	-	-	-	7.9450695×10^{-02}
13	6	2.3	1	-	1	-	-	-	-2.4594529×10^{-02}
14	1	1.13	1.5	0.35	2	1.25	0.5	2	4.5023959×10^{-02}
15	1	1.35	1	0.5	2	1.5	0.5	2	-4.1136286×10^{-02}
16	1	1.75	1.61	0.87	2	1.37	0.642	2	-5.1133761×10^{-03}
17	2	1.5	0.75	0.75	2	0.75	0.75	2	-9.3313650×10^{-02}

V. ASSESSMENTS

Available ideal-gas isobaric-specific data of Hulse et al. [6] is used to assess the new EOS and other relations. The data have a wide temperature range of 100–1000 K with 11 points. Fig. 3 shows the deviation of the ideal-gas isobaric-specific heat from the new EOS. The new EOS can represent more accurately than the other relations. This deviation pattern indicates that the new EOS has an accurate and reliable representation over a wide range. The deviation pattern of the data of Hulse et al. [6] is close to 0% in a temperature range of 100–1000 K. The EOS has an AAD of 0.17%, a MAX of 0.26%, and an STD of 0.19% against the data of Hulse et al.

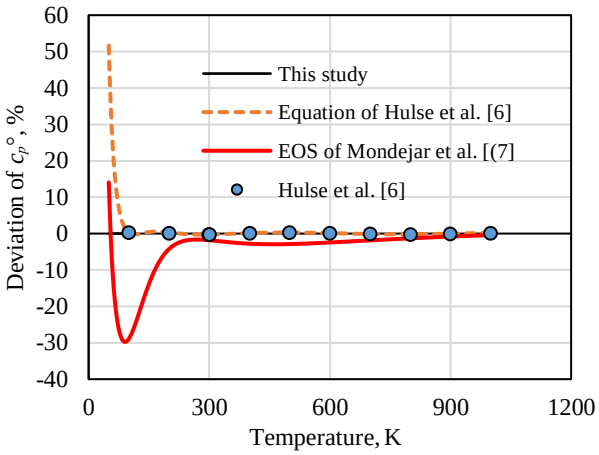

Fig. 3 Deviation of the ideal-gas isobaric-specific heat

The vapor pressure, saturated liquid, and saturated vapor densities are statistically and visually validated. The deviation pattern assessment of experimental data from the calculated results of the EOS is a method used to evaluate the accuracy and reliability in predicting the thermodynamic saturation properties. Figs. 4–6 show the deviation patterns of the vapor pressure, saturated liquid density, and saturated vapor density.

The deviations of the vapor pressure data and the calculated values from the available equation and the new EOS are shown in Fig. 4. Four sources of the experimental data are included inside. A significant difference exists at lower temperatures with the EOS of Mondejar et al. [7]. Vapor pressure calculated from the EOS of Mondejar et al. gives smaller values at a lower temperature. The ancillary equation of the vapor pressure still has a high approach to the new EOS. The adequate amount and spread over a wide temperature range of the data are available with satisfying distribution but poorly distributed near the triple point. Twenty-three-point data of Mondejar et al. [7] has a temperature range of 280–438 K. The statistical analysis results show that the data can be represented with an AAD of 0.53%, a MAX of 1.4%, and an STD of 0.62%. The data of Hulse et al. [6] and Raabe [12] can be represented within an AAD of 2.9% and 5.1%, respectively. Large deviations exist if compared to the experimental data of Nicola et al. [11]. The data of Nicola et al. has a range close to the triple point and a significantly different value from the EOS of Mondejar et al. The new EOS has relatively better accuracy than the correlation existing at low temperatures.

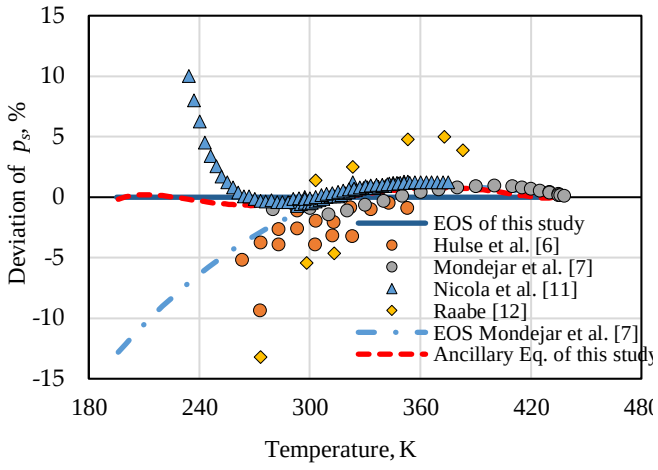

Fig. 4 Deviation of the vapor pressure

The deviation of the saturated liquid density to the calculation results of the EOS is shown in Fig. 5. Two experimental data sources, which have a range of 243–

383 K, are compared. The saturated liquid density of Hulse et al. [12] and Raabe [12] have an AAD of 0.12% and 0.23%, a MAX of 0.36% and 0.65%, and a STD of 0.089% and 0.32%, respectively. Both deviation patterns from the two experimental data sources show relatively good results. The deviation patterns formed from two other correlation results perform significantly differently close to a critical point. The deviation patterns by the two correlations increase as a difficulty fitting process near the critical point.

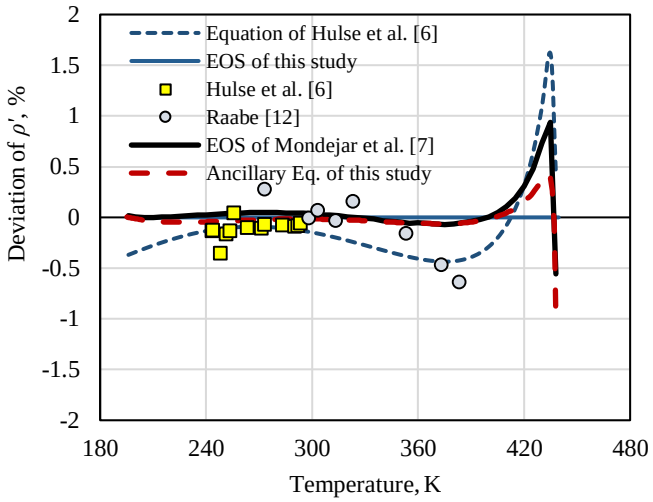

Fig. 5 Deviation of the saturated liquid densities

Available data points for the saturated vapor density are very scarce, which are 8 points only in a range of 273.15–383.15 K from Raabe [12]. This data has an AAD of 4.1%, a MAX of 13%, and an STD of 5.5% from the new EOS, which its deviation pattern is shown in Fig. 6. More experimental data are needed to assess the saturated vapor density. However, in a range of 300–438 K, both EOS have relatively similar characteristics, except at a temperature lower than 300 K. This increasing deviation dues to the absence of experimental data near the triple point. It means that both EOS still needs to be examined for the saturated vapor density at the lower temperatures. However, the new EOS represents lower vapor pressure deviation at low temperatures and higher vapor pressure and larger saturated vapor density values. This fact indicates that larger saturated vapor density from the new EOS at low temperatures is more reasonable.

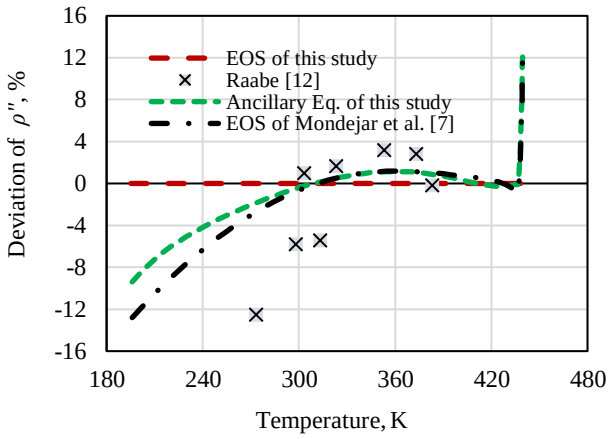

Fig. 6 Deviation of the saturated vapor densities

The visualization and statistical analysis can reveal the density deviation in the single phase. The data points in the supercritical region are included either in the vapor or liquid phases. Figs. 7 and 8 show fairly good deviation patterns of the density. Most experimental data show a low deviation. Most deviation in the liquid phase is smaller than in the vapor phase. The highest deviation pattern occurs near the critical point to represent Tanaka data [13]. These densities have a temperature range of 328.5–438.55 K and a pressure range of 0.7768–9.7651 MPa with an AAD of 0.54%, a MAX of 5.7%, and an STD of 1.1%. Apart from Tanaka's data, there are also experimental data from Fedele et al. [14], Mondejar et al. [7], and Romeo et al. [15] within an AAD of 0.032%, 0.059%, and 0.045%, respectively.

Fig. 8 shows a larger density deviation pattern in the vapor than in the liquid phase. The largest deviation existing in the critical region due to the larger uncertainty data causes it harder to fit. The data of Tanaka [13], which is near critical point and has a temperature range of 423.54–443.54 K and a pressure range of 2.5621–8.6316 MPa, is reproduced within an AAD of 5.5%, a MAX of 31%, and an STD of 7.5%. Two other data sources of the vapor density have lower temperatures and pressures than Tanaka's data. Both data are Fedele et al. [14] and Mondejar et al. [7] within an AAD of 0.26% and 0.13%, respectively.

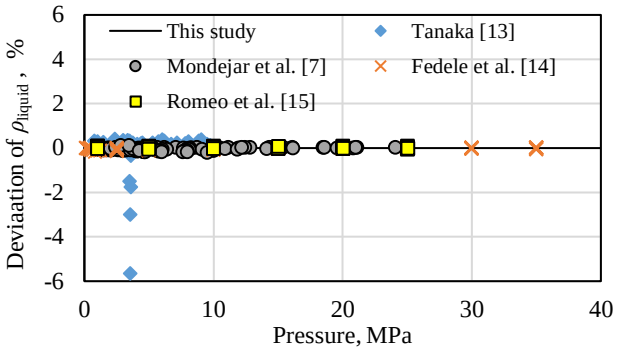

a) Deviation respect to pressure

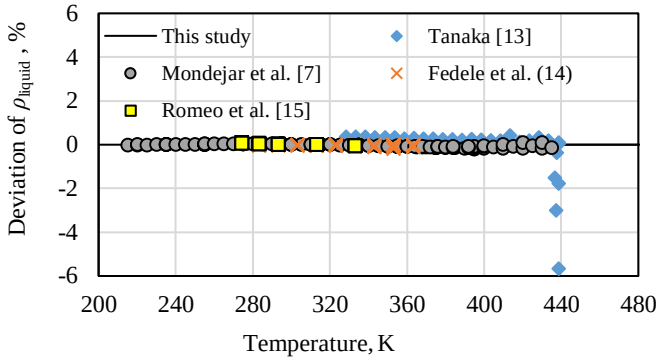

b) Deviation respect to temperature

Fig. 7 Deviation of the liquid densities

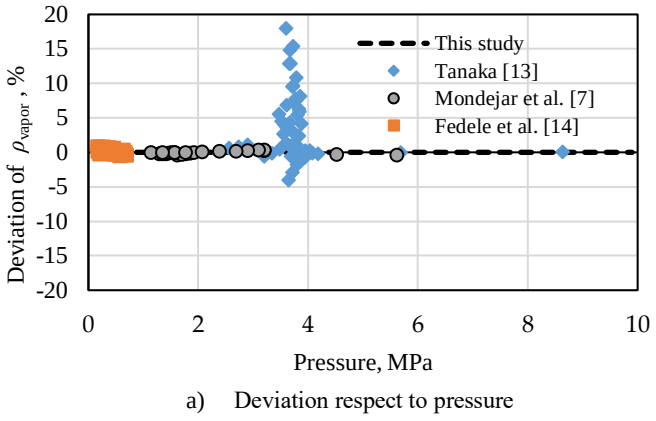

a) Deviation respect to pressure

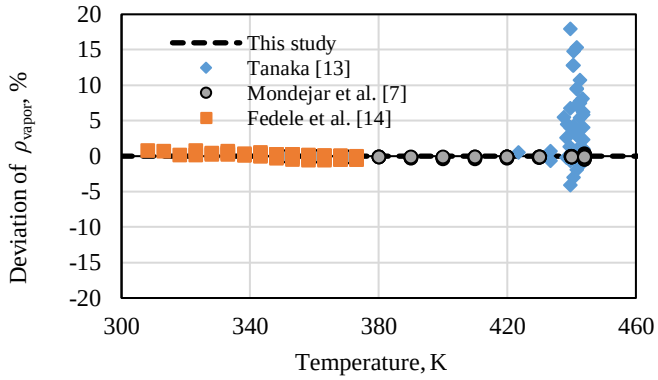

b) Deviation respect to temperature

Fig. 8 Deviation of the vapor densities

Currently, the isochoric specific heat and saturated specific heat data are unavailable. Therefore, these data are not assessed. Isobaric specific heat was obtained from one data source, namely Liu and Zhao [16]. Liu and Zhao reported 63 points for the temperature of 313.277–445.857 K and pressure of 1.02–10.1 MPa. Among the data, only 6 points are in the vapor phase while the others are in the liquid phase. The deviation pattern of these data is shown in Fig. 9. Liu and Zhao's data have an AAD of 3.6% and a MAX of 8.9%.

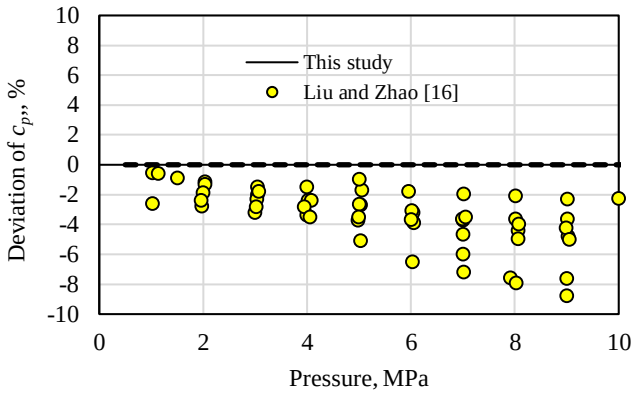

a) Deviation respect to pressure

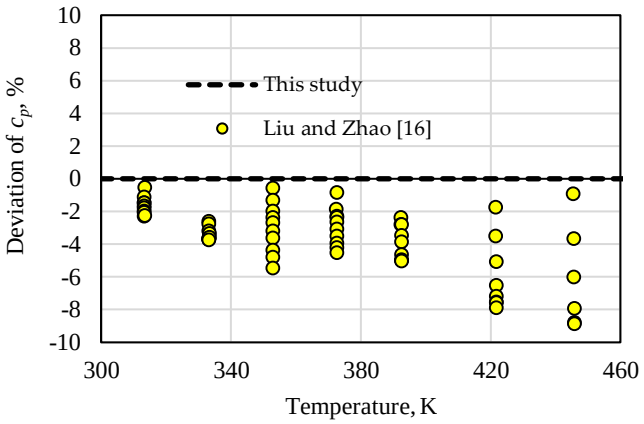

b) Deviation respect to temperature

Fig. 9 Deviation of the isobaric specific heat

Evaluation of the speed of sound was conducted in the liquid and vapor phases. The reason is that the speed-of-sound data in the liquid phase has higher uncertainty than in the vapor phase. The deviations of the sound-of-speed for the vapor and liquid phases are presented visually concerning the pressure and temperature shown in Figs. 10 and 11, respectively. The EOS represents the vapor phase data of Mondejar et al. [7], which has 155 points with a temperature range of 289.99–419.70 K and a pressure range of 0.06835–2.07287 MPa, with an AAD of

0.18% and a MAX of 0.60%. On the other hand, the liquid phase data of Lago et al. [17], which has 43 points with a temperature range of 273.15–353.15 K and a pressure range of 0.3–35 MPa, are reproduced within an AAD of 0.15% and a MAX of 0.43%. The proper behavior of the speed of sound data is that accuracy in the vapor phase is better than in the liquid phase. Therefore, the new EOS has the same relative reliability in predicting the speed of sound in the vapor and liquid phases.

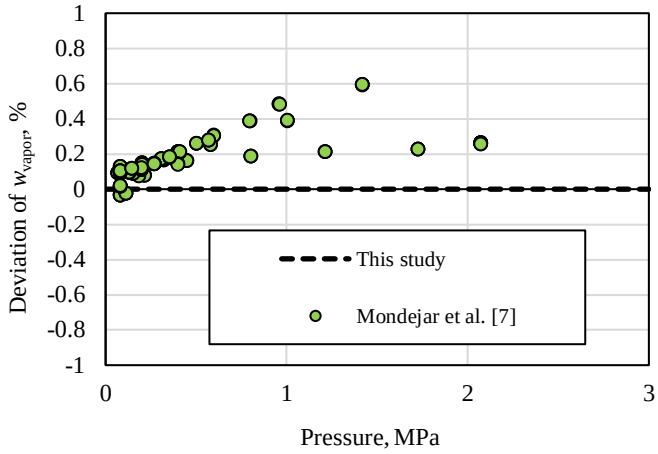

a) Deviation respect to pressure

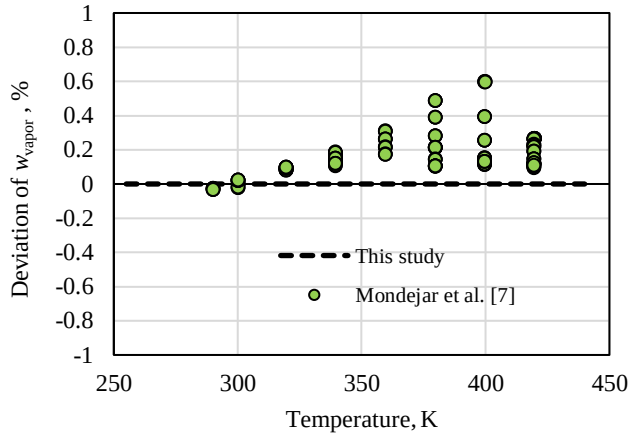

b) Deviation respect to temperature

Fig. 10 Deviation of speed of sound in the vapor phase

Extrapolation of the pressure-temperature-volume properties derived from the new EOS has a temperature range of 196–1000 K and a pressure range of 0.0001–100 MPa as shown in Fig. 12, but the available data ranges are 215–444 K and 0.133–35 MPa. Its isothermal lines behavior shows proper extrapolation.

Extrapolation of the isochoric specific heat for the same range shows good behavior as shown in Fig. 13. The isochoric specific heat value increases with increasing the temperature and pressure. In the region below the critical point the changes of the isochoric specific heat value due to changes in the liquid into the vapor. High isochoric specific heat from the liquid phase changes to low when it enters into the vapor phase, so that vertical lines are formed in two-phase. Good reliability of the new EOS is also performed in the results of isobaric lines near the critical point. The isochoric specific heat values increase significantly near the critical point.

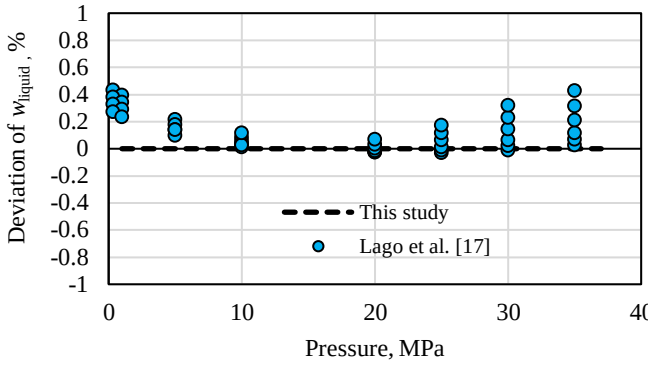

a) Deviation respect to pressure

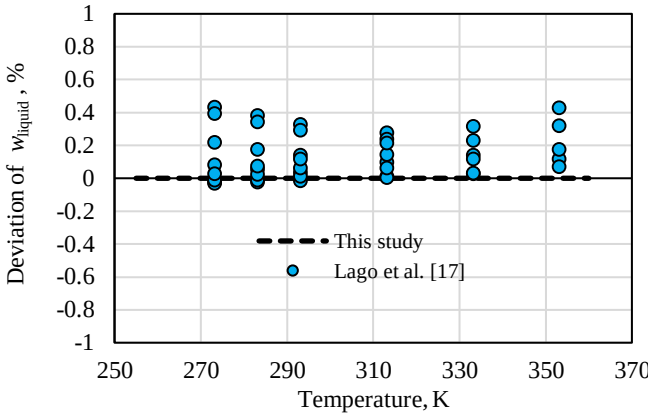

b) Deviation respect to temperature

Fig. 11 Deviation of speed of sound in the liquid phase

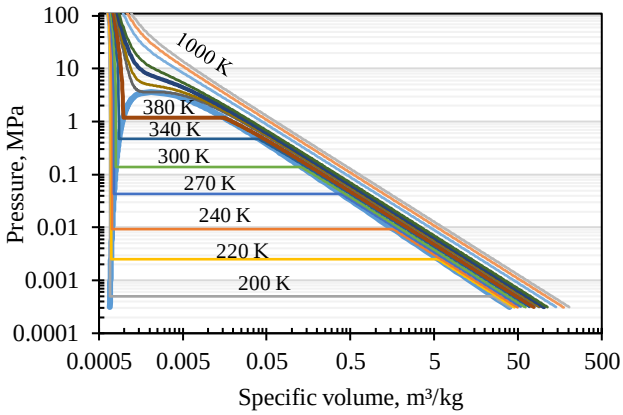

Fig. 12 PVT Extrapolation behavior

Similar trend is also performed for isobaric lines of the isobaric specific heat, but it is on a different scale as shown in Fig. 14. Gradient of isobaric specific heat is smaller than the isochoric specific heat at the same pressure and temperature. However, the isobaric specific heats have larger value at critical region than the isochoric specific heats.

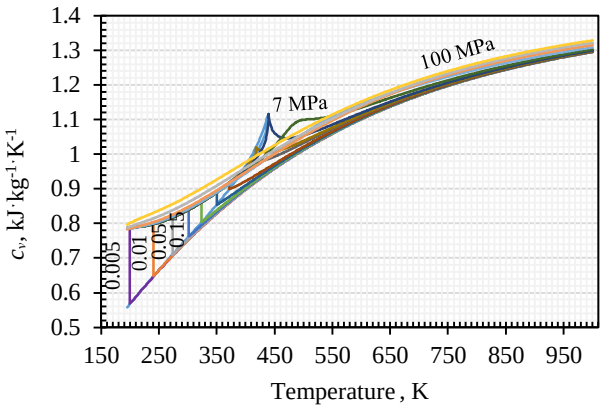

Fig. 13 Isochoric specific heat extrapolation behavior

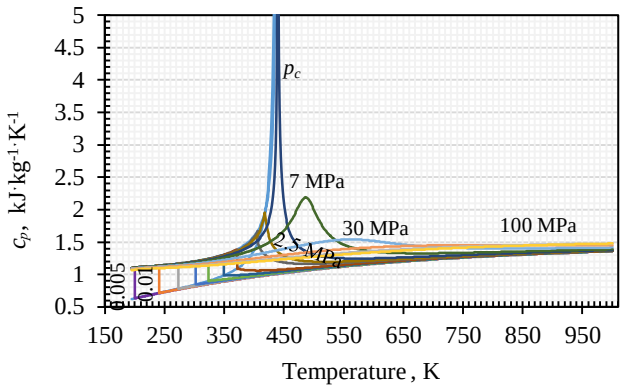

Fig. 14 Isobaric specific heat extrapolation behavior

The extrapolation result of the speed-of-sound values derived from the EOS also shows good behaviors as shown in Fig. 15. The speed-of-sound values at isobaric lines becomes lower at high temperatures. Its value is high at low temperatures because the substance particles are close together so that the sound can be better transmitted. In contrast to high temperatures, the speed of sound decreases because the density of the particles becomes looser. The lower particle density makes it more difficult for sound to propagate. The phase change from liquid to vapor causes the speed of sound significantly decreased. Larger pressure at the same tempearture also contributes to increase the speed-of-sound value.

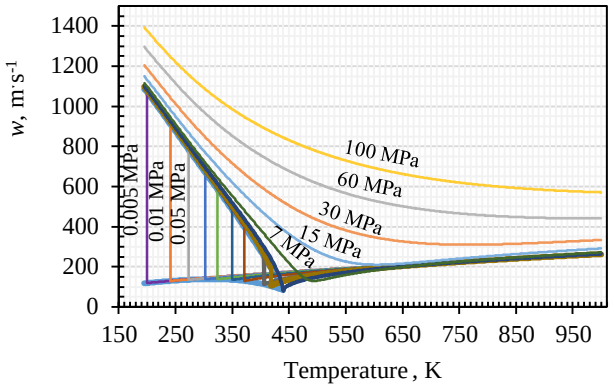

Fig. 15 Speed of sound extrapolation behavior

The characteristic curve is one type of evaluation is derived to assess the ability to extrapolate values of the properties from an EOS. The characteristic curves consisting of the ideal gas, the Boyle, the Joule inversion, and the Joule-Thomson inversion are incorporated in this assessment. The characteristic curves derived from the new EOS and Mondenjar et al. [7] EOS are shown in Fig. 16. The pattern of the characteristic curves is to meet the general curve shape as a curved line. The curvature of the continuous and even characteristic curve shows that the EOS has good reliability to extrapolate. In addition, the ideal-gas and Boyle curves must form an asymptote at the same temperature value [21]. All of these conditions achieved by the curves indicate that the new EOS has the reliable extrapolation for a wide range as a performed range in the curves. The EOS of Mondejar et al. has difficulty closing the curves at higher temperatures.

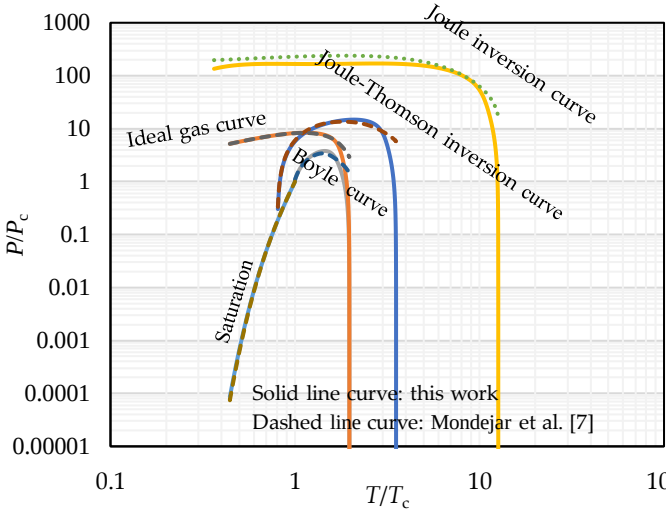

Fig. 16 Ideal characteristic curve from the new EOS

The second and third virial coefficients derived from the new EOS and other equations are shown in Figs. 17 and 18. Accuracy of the calculation values is not the essential goal, but the pattern yielded from the equation and EOS is the goal to be achieved. The second virial values derived from an equation of Pitzer and Curl [22] and an EOS of Mondejar et al. [7] are incorporated in this assessment. The curvature of the second virial coefficient curves towards the negative direction at a low temperature value, but the value achieved is not lower than the virial coefficient from the results of the other equation calculations. The same tendency is also indicated by the second virial coefficient of this study, which have curves in the negative direction at low temperatures. The curve tendency then moves closer to the zero value line at high temperatures. It means that the second virial coefficient derived from the new EOS meets the expected curve pattern.

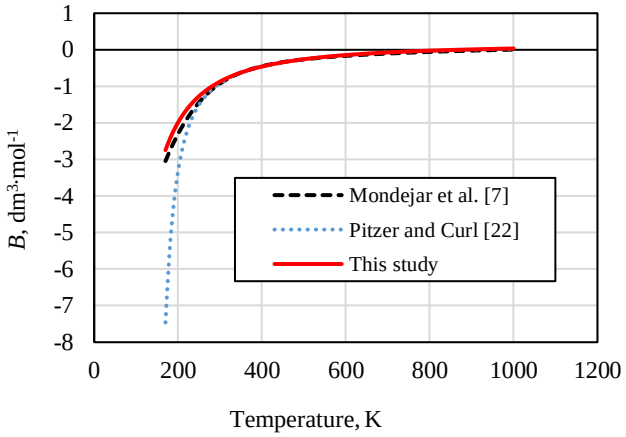

Fig. 17 Comparison of second virial coefficient behaviors

The behavior of the third virial coefficients is clarified to be consistent EOS behavior as changing temperatures at the lowest density. Similar to the main objective of this assessment with the second virial coefficient, the third virial coefficient must also perform a negative curve pattern at low temperatures and towards zero at high temperatures. The overall goal can be achieved using the new EOS. The results of this study are also different from the results of the EOS of Mondejar et al. [7] but closer to Orbey and Vera equation [18].

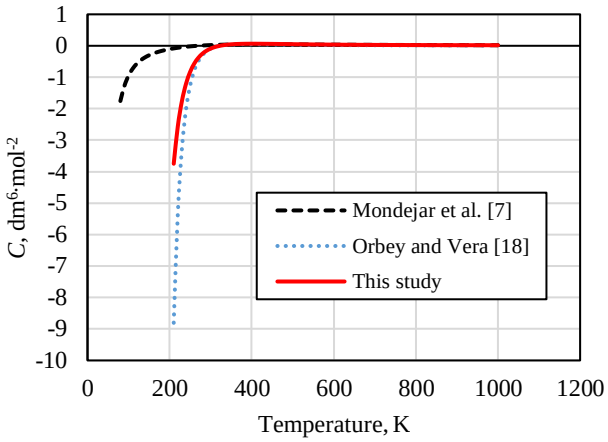

Fig. 18 Comparison of third virial coefficient behaviors

VI. CONCLUSION

The EOS for R-1233zd(E) was developed and represented in Helmholtz free energy. It is divided into two parts, i.e. an ideal gas part and a residual part, and completed with three ancillary equations consisting of equations for the vapor pressure and the saturated liquid and vapor densities. The EOS reproduces the experimental data with an AAD of 0.12% for the liquid density, 2.0% for the vapor density, 1.4% for the vapor pressure, 0.16% for the saturated liquid density, 4.1% for the saturated vapor density, 3.6% for the isobaric specific heat, and 0.15% for the speed of sound in the liquid phase, and 0.18% for the vapor phase. The isochoric and saturated specific heats were not assessed due to unavailable experimental. Reasonable behaviors of the extrapolation and the ideal characteristic curves derived from the EOS clarify its reliability. The EOS can be used to predict thermodynamic properties from the triple point to 1000 K and 100 MPa. The EOS mostly represents more accurately than the previous existing EOS.

VII. REFERENCES

[1] European Fluorocarbons Technical Committee (EFCTC), "Climate Change & The Green Deal," [Online]. Available: https://f-gas-regulation-review-2022.eu/climate-change-the-green-deal/. [Accessed 08 January 2021].

[2] EFTC, "Fluorocarbons: Substance and Main Application," European Fluorocarbons Technical Committee, 1 11 2018. [Online]. Available: https://www.fluorocarbons.org/wp-content/uploads/2020/10/Fluorocarbons-Molecules-2018-November-v2.pdf. [Accessed 31 01 2022].

[3] European Fluorocarbons Technical Committee (EFCTC), "HCFO-1233zd(E) Chillers Receive Environment Awards

Around the World," 20 January 2020. [Online]. Available: https://www.fluorocarbons.org/news/hcfo-1233zde-chillers-receive-environment-awards-around-the-world/. [Accessed 30 Dec 2020].

[4] T. Schmidt, R. Bertermann, G. M. Rusch, A. Tveit and W. Dekant, "Biotransformation of trans-1-chloro-3,3,3-trifluoropropene (trans-HCFO1233zd)," Toxicol Appl Pharmacol., vol. 268, pp. 343–351, 2013.

[5] N. Miyoshi, R. Suemitsu, Y. Togano, Y. Kanki and Y. Hasegawa, "Centrifugal Chiller Using HFO-1233zd(E)," in JRAIA International Symposium, 2016.

[6] R. J. Hulse, R. S. Basu, R. R. Singh and R. P. H. Thomas, "Physical Properties of HCFO-1233zd(E)," Journal of Chemical and Engineering Data, vol. 57(12), pp. 3581–3586, 2012.

[7] M. E. Mondejar, M. O. McLinden and E. W. Lemmon, "Thermodynamic Properties of trans-1-Chloro-3,3,3-Trifluoropropene (R1233zd(E)): Vapor Pressure, (p, ρ, T) Behavior, and Speed of Sound Measurements, and Equation of State," Journal of Chemical and Engineering Data, 60(8), vol. 60, no. 8, pp. 2477–2489, 2015.

[8] H. Zhang, B. Gao, H. Li, Y. Zhao, W. Wu, Q. Zhong, X. Dong, Y. Y. Chen and M. Gong, "Saturated Liquid Density Equation for Pure Refrigerants Including CFCs, HCFCs, HFCs, HCs, HFOs, HFEs, PFAs and ISs Based on The Scaling Law and The Law of Rectilinear Diameter," International Journal of Refrigeration, vol. 87, pp. 65–77, 2018.

[9] ChemScr, "(1E)-1-Chloro-3,3,3-trifluoro-1-propene," ChemSrc, 19 01 2022-01. [Online]. Available: https://www.chemsrc.com/en/ cas/102687-65-0_1044358.html. [Accessed 31 01 2022].

[10] E. Tiesinga, P. J. Mohr, D. B. Newell, and B. N. Taylor, CODATA Recommended Values of the Fundamental Physical Constants: 2018, Journal of Physical and Chemical Reference Data, 50(3): 033105, 2021.

[11] G. D. Nicola, C. Brandoni, C. D. Nicola and G. Giuliani, "Triple Point Measurements for Alternative Refrigerants," Journal of Thermal Analysis and Calorimetry, vol. 108, pp. 627–631, 2012.

[12] G. Raabe, "Molecular Simulation Studies on the Vapor–Liquid Equilibria of The cis- and trans-HCFO-1233zd and The cis- and trans-HFO-1336mzz," Journal of Chemical and Engineering Data, vol. 60, no. 8, pp. 2412–2419, 2015.

[13] K. Tanaka, "pρT Property of trans-1-Chloro-3,3,3-Trifluoropropene (R 1233zd(E)) near Critical Density," Journal of Chemical and Engineering Data, vol. 61, no. 10, pp. 3570–3572, 2016.

[14] L. Fedele, M. Pierantozzi, G. D. Nicola, J. S. Brown and S. Bobbo, "Compressed Liquid Density and Vapor Phase PvT Measurements of trans-1-Chloro-3,3,3-trifluoroprop-1-ene [R1233zd(E)]," Journal of Chemical and Engineering Data, vol. 63, no. 1, pp. 225–232, 2018.

[15] R. Romeo, P. A. G. Albo, S. Lago and J. S. Brown, "Experimental Liquid Densities of cis-1,3,3,3-Tetrafluoroprop-1-ene (R1234ze(Z)) and trans-1-Chloro-3,3,3-Trifluoropropene (R1233zd(E))," International Journal of Refrigeration, vol. 79, pp. 176–182, 2017.

[16] Y. Liu and X. Zhao, "Measurement of The Heat Capacity of R1233zd(E)," International Journal of Refrigeration, vol. 86, pp. 127–132, 2018.

[17] S. Lago, P. A. G. Albo, J. S. Brown and M. Bertinetti, "High-Pressure Speed of Sound Measurements of trans-1-Chloro-3,3,3-trifluoropropene (R1233zd(E)) in Liquid Region for Temperature from (273.15 to 353.15) K," Journal of Chemical and Engineering Data, vol. 63, no. 11, pp. 4039–4045, 2018.

[18] H. Orbey and J. H. Vera, "Correlation for the Third Virial Coefficient Using Tc, Pc, and ω as Parameters," Journal of the American Institute of Chemical Engineers, vol. 29, no. 1, pp. 107–113, 1983.

[19] I. M. Astina and H. Sato, "A Rapid Genetic Optimization Technique for Rational Thermodynamic Modeling Having Reliable Third Virial Coefficients," in International Conference of Thermophysics, Boulder, 2002.

[20] I. M. Astina, G. Budiarso and R. Harrison, "New Helmholtz Equation of State for HFO-1234ze (E) with Comprehensive Assessment," Fluid Phase Equilibria, vol. 531, no. 112921, 2021.

[21] U. K. Deiters and A. Neumaier, "Computer Simulation of the Characteristic Curves of Pure Fluids," Journal of Chemical and Engineering Data, vol. 61, no. 8, pp. 2720–2738, 2016.

[22] K. S. Pitzer and R. F. Curl Jr., "The Volumetric and Thermodynamic Properties of Fluids. III. Empirical Equation for the Second Virial Coefficient," Journal of the American Chemical Society, vol. 79, no. 10, pp. 2369–2370, 1957.

[23] J. Majurin, E. Sorenson, D. Steinke and M. Herried, "Chemical Stability Assessments of R-514A and R-1233zd(E)," ASHRAE, 2017.

Cite this Article

Galih Budiarso, I Made Astina, "Development of Helmholtz Equation of State for Thermodynamic Properties of R-1233zd(E)", International Journal of Scientific Research in Science and Technology (IJSRST), Online ISSN: 2395-602X, Print ISSN: 2395-6011, Volume 9 Issue 3, pp. 765–776, May-June 2022. Available at doi : https://doi.org/10.32628/IJSRST2293148

Journal URL : https://ijsrst.com/IJSRST2293148